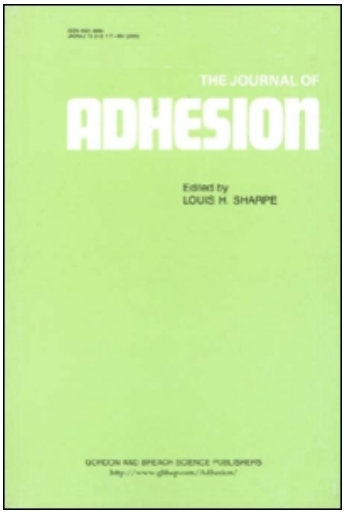

The Journal of Adhesion
Publication details, including instructions for authors and subscription information:
http://www.informaworld.com/smpp/title~content=t713453635

Surface Modification of Polycarbonate by Ultraviolet Radiation and Ozone

Alekh S. Bhurke[a]; Per A. Askeland[a]; Lawrence T. Drzal[a]
[a] Composite Materials and Structures Center, Michigan State University, East Lansing, Michigan, USA

To cite this Article Bhurke, Alekh S. , Askeland, Per A. and Drzal, Lawrence T.(2007) 'Surface Modification of Polycarbonate by Ultraviolet Radiation and Ozone', The Journal of Adhesion, 83: 1, 43 — 66
To link to this Article: DOI: 10.1080/00218460601102860
URL: http://dx.doi.org/10.1080/00218460601102860

The Journal of Adhesion, 83:43–66, 2007

ISSN: 0021-8464 print/1545-5823 online
DOI: 10.1080/00218460601102860

Taylor & Francis
Taylor & Francis Group

Surface Modification of Polycarbonate by Ultraviolet Radiation and Ozone

Alekh S. Bhurke
Per A. Askeland
Lawrence T. Drzal
Composite Materials and Structures Center, Michigan State University, East Lansing, Michigan, USA

The effect of ultraviolet (UV) radiation in the presence of ozone as a surface treatment for polycarbonate is examined in regards to changes in the wettability, adhesion, and surface mechanical properties. Standalone, 175-μm-thick films of a commercially available polycarbonate were exposed to UV radiation from sources of different power with various treatment times in the presence of supplemental ozone. Significant decreases in the water contact angle were observed after exposure to UV radiation in the presence of ozone. After several variations in the experimental setup, it was determined that the change in water contact angle is a function of the UV irradiance and the work of adhesion follows a master curve versus UV irradiance. Nanoindentation experiments revealed that the modulus of the top 500 nm of the surface is increased following UV exposure, attributable to surface cross-linking. Adhesion tests to the surface (conducted by a pneumatic adhesion tensile test instrument) showed little change as a function of UV exposure. Analysis of adhesion test failure surfaces with X-ray Photoelectron Spectroscopy (XPS) showed the locus of bond failure lay within the bulk polycarbonate and the measured bond strength is limited by the bulk properties of the polycarbonate and/or the creation of a weak boundary layer within the polymer.

Keywords: Adhesion; Ozone; Polycarbonate; Surface energy; Surface treatment; Ultraviolet

1. INTRODUCTION

Adhesive bonding of metals, polymers, and polymer composites is an attractive structural fabrication method, creating strong, stable joints

Received 17 July 2006; in final form 13 October 2006.

Address correspondence to Lawrence T. Drzal, Composite Materials and Structures Center, 2100 Engineering Building, Michigan State University, East Lansing, MI 48824-1226, USA. E-mail: drzal@egr.msu.edu

with superior mechanical properties and durability as compared with mechanically fastened structures. The application of protective coatings and paints to surfaces is also an important manufacturing process in the durable goods industry. In such processes, the surface preparation of the substrate is an important step. Polymers and polymer composites often have low surface energies and may also contain processing additives that can reduce or limit adhesion. Surface preparation of the adherend for adhesive bonding or painting often involves removal of adhesion limiters such as surface contamination, poor mechanical conditions such as weak boundary layers, and the addition of active chemical functionalities that can interact strongly with the adhesive or paint.

Various mechanical and chemical surface treatments have been developed to overcome the problem of weak adhesion in polymers. Mechanical surface treatments such as abrasion can be time consuming, labor intensive, and damaging to the substrate. Organic solvents are often used for cleaning surfaces but present various environmental problems, and the role of many traditionally used solvents is being reduced or eliminated by a combination of legislation and growing environmental awareness. Other surface treatment techniques such as flame, plasma, and corona discharge have also been developed [1–9]. Although these surface treatments are efficient and used widely in industry, they suffer from drawbacks such as high cost, hazardous operating conditions, by-products, and the inability to treat complex geometric shapes. There is a growing need in industry for a fast, simple, efficient, and environmentally friendly surface treatment process that can be easily incorporated into the manufacturing environment [10].

The energy provided by an ultraviolet (UV) photon is often sufficient to induce chemical changes in the structure of many polymers. Exposure of oxygen to 185 nm of UV radiation creates an aggressive oxidizing environment as molecular oxygen absorbs strongly at that wavelength and dissociates into monoatomic oxygen. Oxygen radicals further react with molecular oxygen to form ozone [11,12]. If a broad spectrum UV source such as a xenon arc lamp is used, UV radiation at 254 nm is also available. Ozone has a strong absorption cross-section at 254 nm and dissociates into oxygen and oxygen radicals, creating a dynamic oxidizing environment, which can effectively remove low-molecular-weight organic contaminants from the surface. Another phenomenon that is responsible for activating the surface, especially in polymers, is the etching and activation of the polymer surface from ablation by high-energy UV radiation [13–17]. On exposure to UV radiation of sufficiently high energy, organic bonds in the surface layer can be rapidly broken, depending on the absorbance of the substrate. When

activated surfaces are exposed to the atmosphere, oxidation takes place with the formation of highly polar surface groups such as hydroxyl, carbonyl, and carboxylic acids, which can improve wettability and adhesion [7,9,12,18–29]. UV light with wavelengths from 184 to 365 nm (UVC radiation) produced by commercially available xenon and low-pressure mercury vapor lamps is ideal for the process of surface activation and oxidation. Exposure of a receptive material to UVC radiation for short times in the presence of oxygen or ozone can yield a surface with high surface energy, wettability, and adhesive strength [30,31]. UV surface treatment also has the ability to treat three-dimensional surfaces because of the line-of-sight nature of the process. The by-products of such processes are largely expected to be water and oxides of carbon. The process does not utilize any solvents, and the ozone is dynamically created and dissociated in the treatment environment.

Though phenomenological studies of the UV interactions with polycarbonate in regards to degradation pathways have been pursued since the early 1970s, there has been little effort to study the UV photoactivation of a surface in conjunction with the photodegradation of ozone as potential surface treatment. In this work, the effects of UV/ozone treatments in regards to changes in wettability, adhesion, and surface toughening of polycarbonate are examined. In particular, a variety of process variables including irradiance, exposure time, ozone concentration, temperature, and humidity are examined. In addition, the changes occurring on the surface are strongly dependent on external mass transfer, nature and surface chemistry of the substrate, and surface chemical reactions. Understanding the process involves a systematic study of these process parameters. In this article, results of studies on the effects of mass transfer, ozone concentration, irradiance, and exposure time are presented.

2. EXPERIMENTAL

2.1. Materials

A commercial-grade bisphenol-A-based polycarbonate (GE Plastics, Pittsfield, MA, USA), GE8040, was used for all samples in this study. The material is available as an extruded film 175 μm thick and is packaged with a protective polymer (polyolefinic) film on both sides. One side of the protective films adheres to the polycarbonate (PC) film by electrostatic attraction while the film on the other side of the polycarbonate adheres with a pressure-sensitive adhesive. Although XPS analysis of the side protected by pressure-sensitive adhesive film did

not show any evidence of transfer of the adhesive to the polycarbonate film, only the side protected by the electrostatically attached film was used in all experiments to avoid the possibility of artifacts. The molecular weight of the polycarbonate used is *ca.* 20,000 Daltons.

The UV surface treatment process involves the oxidation of the material surface with ozone in the presence of UV radiation. Ozone is produced by the interaction of 185-nm wavelength photons with molecular oxygen, and the amount of ozone formed depends on the output of 185-nm radiation [18]. Xenon lamps have significant output at 185 nm and with appropriate selection of the equipment the required ozone can be produced *in situ* during UV treatment. However, reliance on *in situ* production of ozone can present problems during short batch operations such as laboratory experiments because the ozone produced under the lamp may not reach steady-state concentrations immediately on startup. To avoid this problem, an external ozone generator (Ozotech Inc., Yreka, CA, USA), OZ6BTU, was used in experiments requiring ozone to ensure steady-state conditions using pure oxygen feed gas. Ozone produced was introduced in the treatment environment at room temperature and pressure conditions. Another advantage of using an external ozone generator is the ability to independently vary the ozone concentration and flow rate to study their effect on the process. Ozone has a strong absorption maximum at 253.7 nm with a molar extinction coefficient of 0.000308 $ppm^{-1}cm^{-1}$ at 0°C and 1 atm pressure. A Perkin Elmer Lambda 900 UV-Vis-NIR spectrometer (Perkin Elmer, Wellesely, MA, USA) was used to measure the concentration of ozone. The outlet from the ozone generator was connected to the UV treatment chamber, and gas samples from the treatment chamber were transferred via a glass nozzle and ozone-resistant silicone tubing to a 1-mm-path-length quartz flow cell mounted in the spectrometer. Continuous flow of the sample gas through the flow cell was achieved by connecting the outlet of the cell to a small vacuum pump.

2.2. UV Lamps

Three xenon flash lamps (Xenon Corporation, Woburn, MA, USA) operating at frequencies ranging from 3 to 120 Hz were used. The nominal power, frequency, and shape of the lamps are summarized in Table 1. The lamps are equipped with aluminum reflectors and fused quartz windows to provide optimum transmission of broad spectrum UV radiation from 185 nm to 380 nm. The outer surface of the lamp window is considered the area source of UV radiation for all determinations of irradiant energy and is the reference plane for measurement of the distance between the lamp and sample surface.

TABLE 1 Brief Description of the Lamps Used in the UVO Treatments

Lamp	Power (W)	Frequency (Hz)	Bulb shape
Xenon RC 500	300	120	5 inches, (12.7 cm), linear
Xenon RC 740	1500	10	3.5 inches (8.9 cm), coil
Xenon RC 747	1500	3, 120	16 inches (40.6 cm), linear

Samples were UV treated in a chamber made from 1/4-inch (0.64-cm) aluminum plates having exterior dimensions of 8 inch (20.3 cm) (l) × 8 inch (20.3 cm) (w) × 1 inch (1.54 cm) (h). A 4 inch (10.2 cm) × 4 inch (10.2 cm) opening was machined in the top of the chamber to provide a path for illuminating radiation. The opening was closed with Suprasil®, (Hereaus Quartz America, Buford, GA, USA), Dynasil® 2000 (Dynasil, W. Berlin, NS, USA) glass plates during treatment. The chamber was equipped with an inlet and outlet for process gases. The schematic of the experimental setup is shown in Figure 1. Although the use of a chamber is not essential to the UV treatment process, all experiments were performed inside the chamber to ensure controlled, measurable, and repeatable experimental conditions.

2.3. Measurement of UV Radiation

The irradiance at 254-nm wavelength incident on the sample was measured using a radiometer (International Light, IL1700 Research Radiometer Peabody, MA, USA) coupled with a solar blind photodiode detector (International Light, SED 220), a 254-nm narrow-band filter (International Light, NS 254), and a quartz cosine-response filter. The radiometer setup was calibrated with National Institute of Science

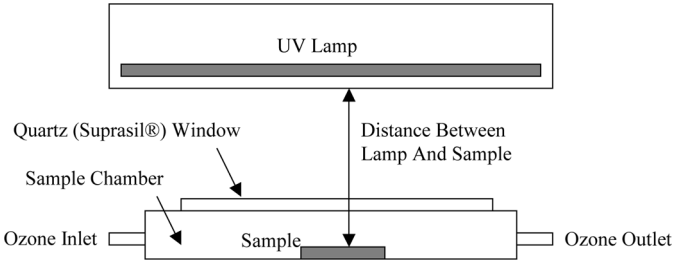

FIGURE 1 UV test chamber constructed from aluminum with a Supracil® quartz window to allow UV transmission. Supplemental ozone is passed through the chamber via gas inlets and outlets.

and Technology (NIST)–traceable standards. To obtain an accurate measure of the amount of radiant energy reaching the sample surface during UV treatment, the entire detector assembly was mounted inside the chamber at the location where samples were mounted for treatment. Irradiance was measured with ozone (approximately 750 ppm) and oxygen gases flowing through the chamber at 30 scfh (standard cubic feet per hour). Irradiation was measured in time-integral mode and the irradiance calculated as the average energy reaching the detector per unit time. Irradiance for RC500 and RC747 lamps was measured as a function of varying distance from the treatment chamber.

2.4. Surface Energy and Surface Chemistry Measurements

Contact angles were measured on a Kruss Drop Shape Analysis System 10 Mk.2 (Kruss, Hamburg, Germany). The instrument has video capture capability to digitize drop shapes. Image analysis was performed using the Drop Shape Analysis software provided with the system. A manual goniometer (Rame-Hart, Mt. Lakes, NJ, USA) was also used to measure contact angles. Contact angles were measured with five liquids of varying acid–base character to calculate the surface energy of modified polycarbonate using the Good–van Oss acid–base model [34,35]:

$$W_{SL} = \gamma_{LV}^{(1+\cos\theta)} = W_{SL}^{LW} + W_{SL}^{AB} = 2\left(\sqrt{\gamma_S^{LW}\gamma_L^{LW}} + \sqrt{\gamma_S^{+}\gamma_L^{-}} + \sqrt{\gamma_S^{-}\gamma_L^{+}}\right).$$

The five liquids used and the acid–base components of their surface energies are given in Table 2. Acid–base parameters of the surface energy were calculated by using the sum of least squares method to fit the five liquid data.

UV-oxidation-induced changes in the surface chemistry were probed with X-ray photoelectron spectroscopy (XPS). UV-treated polycarbonate samples were analyzed with MgKα x-rays in a Perkin Elmer

TABLE 2 Surface Energies of Liquids Used for Contact Angle Measurement

Liquid	γ_L^{Total} (mJ/m^2)	γ_L^{LW} (mJ/m^2)	$\gamma_L^{(+)}$ (mJ/m^2)	$\gamma_L^{(-)}$ (mJ/m^2)	γ_L^{D} (mJ/m^2)	γ_L^{P} (mJ/m^2)
Water	72.80	21.80	25.50	25.50	21.80	51.00
Glycerol	64.00	34.00	3.92	57.40	34.00	30.00
Ethylene glycol	48.00	29.00	1.92	47.00	29.00	19.00
Formamide	58.00	39.00	2.28	39.60	39.00	19.00
Diiodomethane	50.80	50.80	0.00	0.00	50.80	0.00

Phi 5400 ESCA system (Physical Electronics, Chanhassen, MN, USA) at pressures between 10^{-9} and 10^{-8} torr, pass energy of 29.35 eV, and a 45° take-off angle.

2.5. Adhesion Measurements

Stub-pull tensile tests (ASTM D4541) were used to measure adhesive bond strength. A pneumatic adhesion tensile testing instrument (PATTI, M.E. Taylor Engineering, Brookville, MD, USA) was used to measure the pull-off strength of an aluminum stub adhesively bonded to treated surfaces with a structural epoxy (Araldite 2015, Vantico, East Lansing, MI, USA). Figure 2 is a schematic representation of the PATTI test configuration. In the case of thin film or flexible samples, the entire sample is first mounted on a rigid metallic or wooden base prior to testing to prevent sample bending during tensile testing. This is necessary because any bending deformation in the sample can lead to the generation of strong peeling forces at the adhesive interface. Tensile pull-off strength is measured by applying pneumatic pressure, and the failure load is measured. Failure stress is calculated from the peak load.

An alternate stub-shear adhesion test was also developed to measure adhesion on very thin polycarbonate films, which can detach from the stiff base material easily during tensile testing. The sample configuration is identical to that described for tensile stub-pull tests, but the loading is pure shear as shown in Figure 3. Shear tests were performed on a United Testing Systems (Bath, Ohio) mechanical

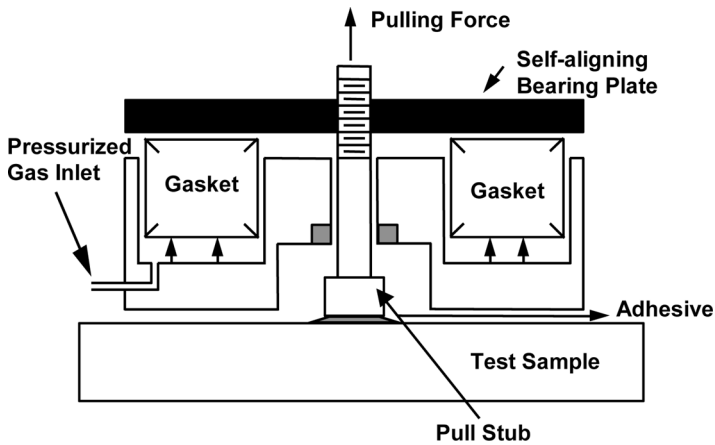

FIGURE 2 Schematic representation of the tensile stub-pull (PATTI) test.

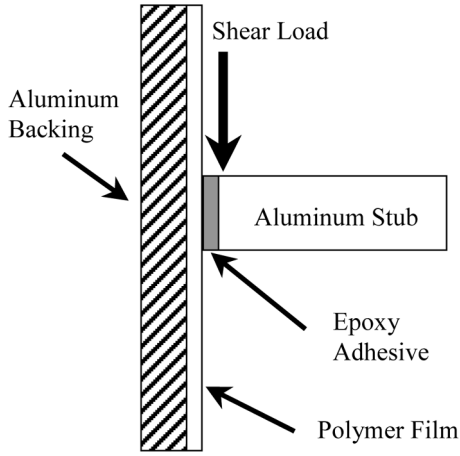

FIGURE 3 The sample configuration for the stub-shear adhesion test.

testing machine with a strain rate of 0.05 inch/minute (0.13 cm/mi-minute). Failure load and stress were measured. The tested surfaces were examined to determine the locus of failure. The failure mode can be either interfacial or substrate. Interfacial failure is seen in cases where the interface between the sample and the adhesive is weak, whereas substrate failure is generally seen when the interfacial adhesion is very high compared with the strength of the bulk substrate, and cohesive failure occurs in the bulk material.

2.6. Nanoindentation

Nanoindentation tests were developed for the purpose of probing the mechanical properties of very small volumes of materials. It is an ideal technique for the characterization of thin films, coatings, and surface layers. The advantage of nanoindentation tests is that material properties in the top 1–2 μm of the substrate can be measured as a function of depth. A MTS nanoindenter (MTS Systems Corp., Eden Priarie, MN, USA) was used to probe the elastic modulus (E) and hardness (H) of UV-treated surfaces.

A nanoindentation test consists of three main steps. An indenter is pushed into the material surface, causing elastic and plastic deformation in the material up to a predetermined contact depth, h_c. The indenter is held at the indentation depth for a period of time with a constant indenter load. The indenter is subsequently withdrawn, and the elastic deformation in the material is recovered. It is the

elastic recovery that allows the determination of the elastic properties of the surface layers. The indenter used for testing was a diamond Berkovich pyramidal tip with $\beta = 1.034$, $E_i = 1141$ GPa, and Poisson's ratio = 0.07. Poisson's ratios for most polymers range between 0.25 and 0.35. For testing of polymers, which can exhibit large plastic deformations, a series of 36 indents were made in a 6×6 matrix with horizontal and vertical spacing of 50 μm between indents. Indents were made to a depth of 2 μm.

3. RESULTS AND DISCUSSION

3.1. Process Parameters

The reaction of ozone with the UV-irradiated surfaces is a gas–solid reaction, and the overall rate of reaction depends on the relative rates of the surface chemical reaction and the mass transfer of reactive species to the surface. The slowest step in the process is the rate determining step, and for a given chemical reaction, the rate constants cannot be changed easily. The external mass transfer in a gas–solid surface reaction, a measure of the ability to transport reactants to the reaction sites on the surface, is a more easily modified parameter. If the system is mass transfer limited, then the overall rate of the reaction is dependent on the mass transfer coefficient, and an increase in mass transfer results in an increase in the total reaction rate to the limit allowed by the reaction kinetics. To determine if mass transfer limitations existed in the experimental setup, contact angles were measured on samples treated at different flow rates. Flow rates of 10, 20 and 30 scfh were used while keeping the ozone concentration and UV-treatment time constant. When the flow rate is decreased, the gas velocity decreases and the mass transfer coefficient decreases. Any mass transfer limitation in this case would be seen as a reduction in the treatment efficiency and higher than normal contact angles for a set of given treatment conditions as the transport of ozone to the surface is hindered by the slow flow rate.

Figure 4 shows the variation of the contact angles as the flow rate is changed by a factor of three for treatment times ranging from 0 to 90-s of UV exposure. The contact angles for untreated polycarbonate were found to be approximately 90°. After UV/ozone (henceforth abbreviated as UVO) oxidation, the contact angles decrease sharply for treatments as short as 10-s. As the treatment time is increased, the rate of change of contact angles decreases, and angles of less than 20° are obtained after treatments of 90 to 120-s. Further changes in contact angles are difficult to measure accurately. Contact angles

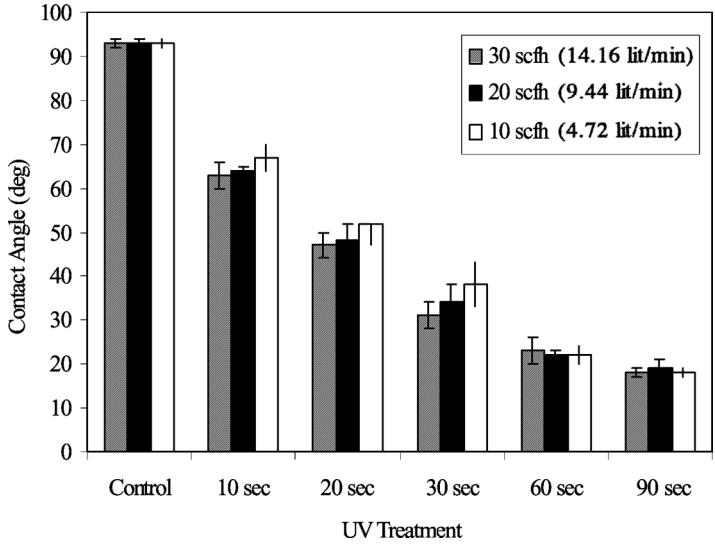

FIGURE 4 Contact angles of UV-treated PC for ozone flow rates of 10, 20, and 30 scfh, indicating no mass transfer limitations.

measured for treatments at all three flow rates were found to be identical within the limits of experimental error and leads to the conclusion that no mass transfer limitation is present when flow rates on the order of 10–30 scfh are used. All further experiments in this article were performed at a flow rate of 30 scfh.

The ozone concentration is a potentially important process variable. Depending on the kinetics of the surface reaction between ozone and the UV-treated surface, the reaction can be strongly dependent on the concentration of ozone on the surface. To determine the influence of ozone concentration on the UV-treatment process, polycarbonate samples were treated at various ozone concentrations at identical operating conditions of irradiance and exposure time. Sessile drop equilibrium contact angles were measured at various locations on multiple samples as shown in Figure 5.

It was found that ozone was necessary for UV treatment, but the concentration of ozone did not have any effect on the quality of treatment achieved. Without additional ozone, contact angles between 70 and 80° were measured for most samples after a 30-s UV exposure. With 400 to 800 ppm ozone in the treatment chamber, contact angles of 30° were obtained for the same exposure. With decreasing ozone concentration, the data show a large amount of variability in the

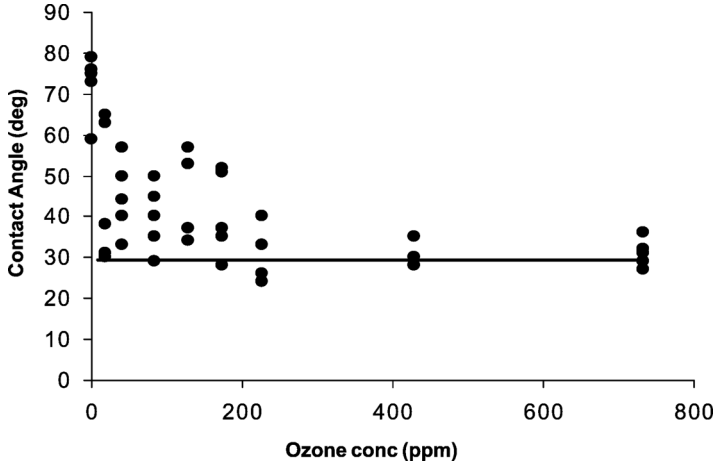

FIGURE 5 Contact angles of PC after 30-s UVO treatment as a function of ozone concentration. Horizontal line indicates the lowest angles measured at the lower limit of measured ozone concentrations.

individual measurements. However, the lowest value of contact angles measured (shown by horizontal line) was *ca.* 30° for all samples irrespective of the ozone concentration. This was observed to be true even at the lower limit (*ca.* 10 ppm) of our capability to measure ozone concentration accurately. In terms of process parameters, UV treatment of PC can be considered to be independent of ozone concentration because, for a surface reaction, ideally only a small amount of ozone is needed to form a monolayer and obtain full surface coverage. To reduce data scatter, ozone concentrations in the range of 700–800 ppm were used for all experimentation.

3.2. Irradiance

The measurement of radiation is broadly classified into two categories: radiometry and photometry [31]. Radiometry is the measurement of energy emitted in a range of wavelengths by a source of radiation, whereas photometry is the measurement of visible light, more commonly concerned with the effect and response of the human eye to light. Radiometric measurement at specific wavelengths of the spectrum or spectral bands is called spectral radiometry. In terms of chemical applications of radiation, spectral radiometry is widely used because chemical reactions often occur at particular wavelengths and the measurement of the amount of radiation emitted at those

wavelengths can be used to quantify the processes. Because of the variety of radiometric units available to quantify radiation, it is important to choose the right unit to describe the system. In an application such as UV surface treatment, the amount of radiation reaching the surface is the quantity of interest, and both intensity and irradiance can be used to quantify the radiation. However, it is important to note that the two units differ in concept: intensity is a unit related to the source of the radiation whereas irradiance is a unit related to the receiving surface. Thus, intensity is more useful in describing the amount of UV radiation emitted by the UV lamp whereas irradiance is more useful in describing the amount of emitted radiation received by a surface exposed to it. Therefore, irradiance is used to quantify radiation in this study.

The relationship between irradiance and distance from a point source is defined by the inverse square law, which states that the irradiance decreases as the square of the distance between the detector and the source [31]. The results of irradiance measurements for the RC500 lamp is shown in Figure 6. The irradiance increases as the distance from the lamp decreases. However, the change in irradiance does not follow the inverse square law exactly because the lamps, far from being point sources, are high-aspect-ratio cylindrical tubes. Additional deviation is caused by the presence of the chamber and window, which limit the angle of view of the detector assembly. This

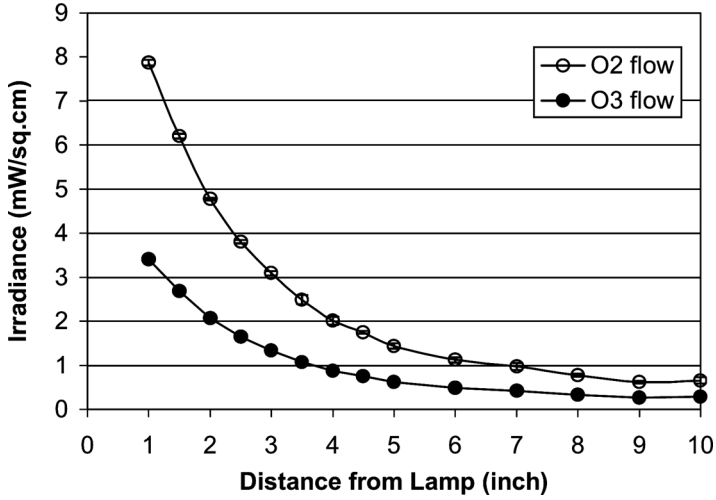

FIGURE 6 Irradiance measurements for RC500 lamp with ozone and oxygen flow.

alleviates the effect of increasing distance as a greater length of the UV lamp is brought into the limited angle of view of the detector as the lamp is moved farther away. The irradiance values obtained also take into account the radiation absorbed by the gas layer (oxygen and ozone) and any reflection and refraction effects from the quartz window and aluminum chamber. The data obtained are a measure of the actual irradiance received by a sample placed in the UV treatment chamber under these specific conditions. Because the irradiance is invariant for a given set of physical conditions, values from the irradiance–distance calibration curves were used for calculating the total irradiation (irradiant energy) received by a sample during treatment such that

$$H = \int_0^t E dt = Et,$$

where H is the irradiant energy or irradiation (J/cm^2), E is the irradiant power or irradiance (W/cm^2), and t is the total UV exposure time (s). The presence of the gas flowing through the chamber has a marked effect on the irradiance. Ozone has a very strong absorption peak at 254 nm, and the incident UV radiation is absorbed by the layer of gas present between the sample and the quartz window. This decrease is absent in the case of oxygen (or air), which has no significant absorption at 254 nm, and consequently higher levels of irradiance were obtained.

Irradiance is the most important variable in the UV-treatment process. The irradiance received by the sample determines the extent of modification possible on the surface. Irradiance levels were measured and varied by controlling the distance between the lamp and sample (however, the path length of ozone the radiation travels through remains constant). Polycarbonate films were exposed to UV radiation from the RC-747 lamp at distances ranging from 1 to 5 inches (2.5 to 12.5 cm) in the presence of approximately 700 to 800 ppm supplemental ozone concentration and a flow rate of 30 scfh. Contact angles of the UV-modified surfaces with deionized water are shown in Figure 7.

As the treatment time is increased, a reduction in contact angles is observed until the contact angles reach 20°, and further reduction in contact angles is difficult to measure accurately as the liquid spreads on the surface. At treatment distances of more than 3 inches (7.6 cm) (irradiance $< 2.6\,mJ/m^2$), the rate of change of the contact angles is almost linear. As the treatment distance is decreased, the increase in irradiance causes the rate of change to be increasingly nonlinear.

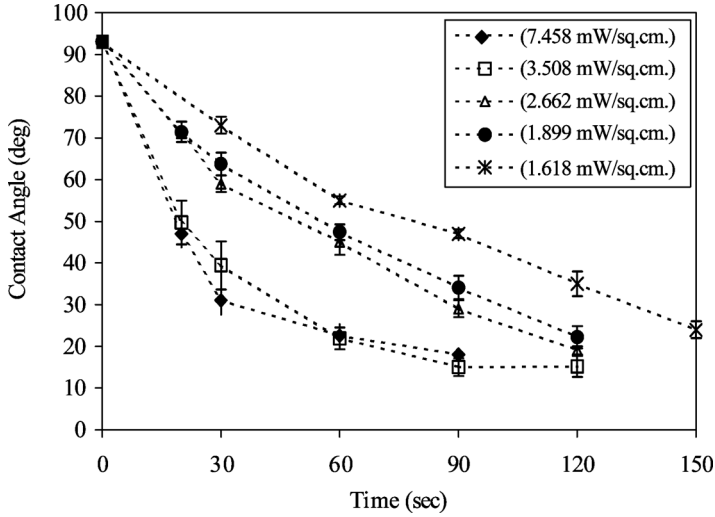

FIGURE 7 Equilibrium contact angles of deionized water on UV-treated polycarbonate as a function of time at various irradiance levels.

It is of particular interest to relate the rate of change of contact angles with an absolute process parameter such as UV irradiance. From observations of the trends in contact angles, it was found that it is possible to superposition the work of adhesion curves for different combinations of irradiance and exposure time. This is similar to the concept of time–temperature superpositioning in polymer creep properties [32]. The time–irradiance superpositioning of the thermodynamic work of adhesion can be expressed as a function of the total irradiation incident on the surface. Figure 7 shows the work of adhesion for deionized water on UV-treated polycarbonate treated at various combinations of distances and UV exposure times. The irradiance was varied by a factor of five, and exposure times of 20 to 150 s were used to generate work of adhesion data. All data in Figure 7 can be reduced to the single curve shown in Figure 8. To test the robustness of this assumption, work of adhesion data were also collected using the low-power RC-500 lamp to create irradiance levels differing by almost an order of magnitude compared with the RC-747 lamp. The data from both lamps follow the superpositioned wettability curve for polycarbonate shown in Figure 8. Acid–base components of the surface energy measured using five liquids of varying acid–base character are shown in Figure 9. As polar functional groups are incorporated on the polymer surface, the wettability and surface energy

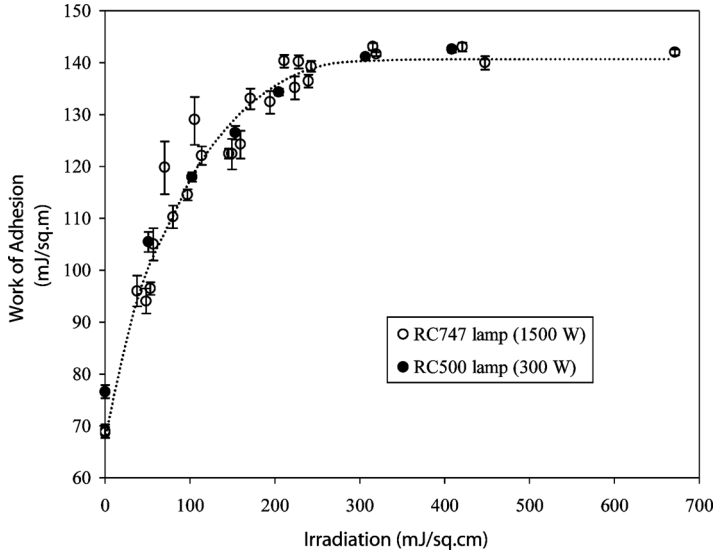

FIGURE 8 Work of adhesion of UV-treated polycarbonate with deionized water as a function of irradiation for data obtained at various combinations of irradiant power and exposure times for multiple lamps.

increases. The surface energy of PC increases from *ca.* 38 mJ/m^2 to 55 mJ/m^2 after UVO treatment. The Lifshitz–van der Waals (39–41 mJ/m^2) and acid (0.5–1 mJ/m^2) contributions remain constant, and most of the increase in surface energy is from an increase in the basic component from 2 mJ/m^2 to 60 mJ/m^2.

XPS analysis was used to quantify the changes in surface chemistry occurring after UVO treatment. Table 3 shows the results of deconvoluted C1s XPS spectra of untreated and UVO-treated polycarbonate. The aliphatic/aromatic carbon peak was assigned at 284.7 eV. Hydroxyl/ether (286.2 eV), carbonyl (287.5 eV), carboxylate/ester (289.8 eV), and carbonate (290.9 eV) peaks were deconvoluted and quantified using Gaussian–Lorentzian statistical fits to the C1s envelope. The results show that UVO treatment leads to an increase in the O/C ratio, indicative of surface oxidation by ozone, and a change in the surface functionality. The total carbonate and hydrocarbon content of the surface decreases with irradiation, indicating chain scission, and hydroxyl, carbonyl, and carboxylate functional groups are incorporated into the surface *via* reactions with ozone. The resultant high-energy, functionalized surface is ideal for bonding with adhesives such as epoxy because of increased wettability and the creation of sites that can form covalent bonds with a reactive adhesive.

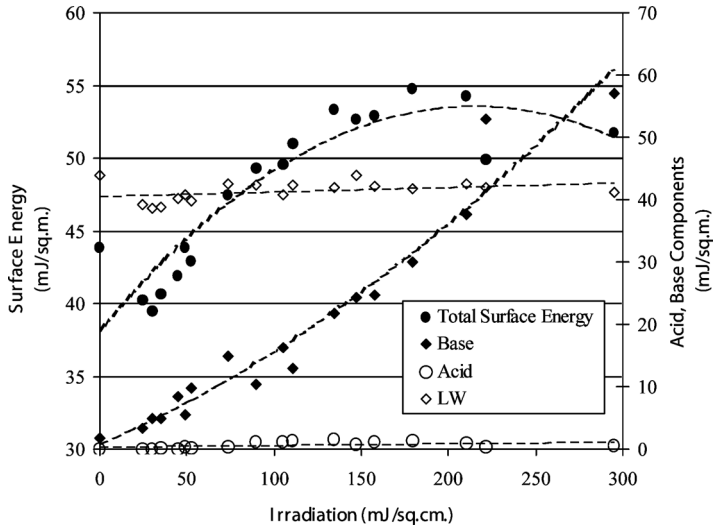

FIGURE 9 Acid–base surface energy of UV-treated polycarbonate for various combinations of irradiance and exposure time.

The construction of a master curve for the change in wettability as a function of irradiation is significant in terms of developing a process model. One of the implications is that time ceases to be a controlling variable in the UV-treatment process, and a specific targeted level of wettability can be achieved by a variety of combinations of irradiance and time. Short treatments at high irradiances and long treatments at low irradiances can yield the same work of adhesion. However, there can be qualitative differences between treatments at high and low

TABLE 3 XPS Surface Chemical Composition of UVO-Treated Polycarbonate

Irradiant energy (mJ/cm^2)	Total carbon (%)	Hydrocarbon[a] (%)	Ether/ hydroxyl[a] (%)	Carbonyl[a] (%)	Carboxyl[a] (%)	Carbonate[a] (%)
0	87.6	73.1	10.0	0.0	0.0	4.5
53	76.8	55.0	11.6	3.9	3.3	3.1
85	76.0	52.2	13.7	3.6	4.6	1.9
120	72.6	44.5	12.1	6.3	6.9	2.8
160	71.0	43.4	13.4	5.9	6.4	1.9
200	68.8	38.9	13.8	7.1	7.9	1.1

[a]Values expressed as percentage concentration of total surface.

irradiances. Surface modification by UV depends on the ability of chromophores in the material to absorb radiation, which is necessary to start a chain of complex reactions. Absorption in the material follows Beer's law, and the intensity of radiation at any point in the thickness of the material depends on the intensity of the incident radiation. Consequently, as irradiance levels are increased to reduce exposure times, the depth at which chemical changes occur in the material can potentially increase. The penetration depth of radiation can thus become an important consideration in choosing combinations of irradiance and time to suit a given application.

3.3. Nanoindentation

Nanoindentation tests on UVO-treated polycarbonate films were performed using a Berkovich pyramidal tip to make 36 indents in the sample surface to a depth of 2000 nm. The spacing between indents was 50 μm, and Poisson's ratio of 0.35 was used for the polycarbonate. Three samples were tested for each treatment condition, and the data for the each sample (36 indents) were averaged separately. Nanoindentation uses the load-displacement data obtained by pushing the diamond tip into the sample surface to calculate surface modulus and hardness. On soft polymer samples, this analysis is complicated by the difficulty experienced by the tip in determining the topmost layer of the surface. The surface is found by the instrument by increasing displacement untill a predetermined load is experienced. Because of the nature of the surface-find segment, properties measured very near the surface have large standard errors. Figure 10 shows the surface modulus of UVO-treated PC as a function of depth up to 500 nm. For both untreated and UV-treated PC, the modulus has a gradient with the highest modulus measured near the surface and a gradual decrease as the probe depth is increased to 2000 nm. The difference in moduli of the top 20–25 nm of the surface for untreated and UVO-treated PC is statistically indeterminate because of the high variability. In spite of the large standard deviations in the top 100 nm of the surface, trends in modulus can be observed as a function of UVO treatment. The untreated material has a modulus between 2.7 and 2.8 GPa in the top 100 nm, which increases to 2.9–3.0 GPa after UV treatment. This trend is seen clearly as the probe depth increases beyond 100 nm. The increase in modulus of the polymer is believed to be due to photo-induced cross-linking of the surface layers. Similar increases in modulus and hardness of physically aged polycarbonate have been reported in the literature and attributed to changes in free volume and chain-scission-induced cross-linking [33].

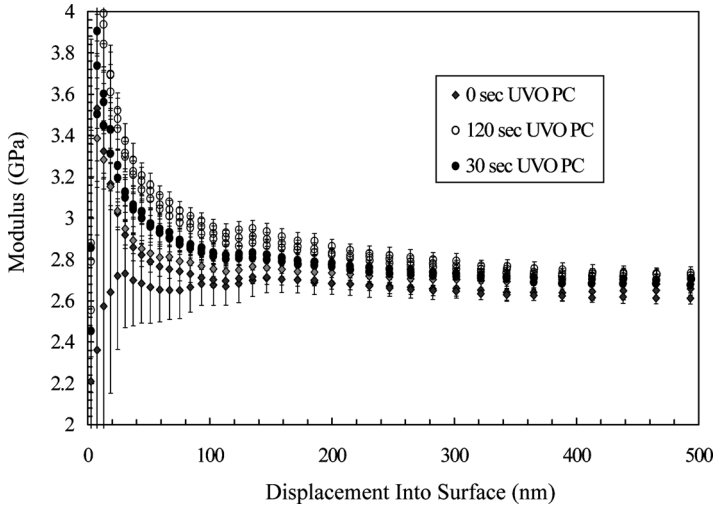

FIGURE 10 Modulus *vs.* depth profiles of UVO-treated polycarbonate measured by nanoindentation tests. Higher modulus in the surface layers is observed with increasing UVO exposure.

3.4. Adhesion

The adhesive performance of UV-treated polycarbonate was measured using two adhesion tests: tensile stub-pull and stub-shear. Tensile tests used a pneumatic piston to pull off an aluminum stub bonded to the PC film, and the failure load was recorded. Shear tests were performed on similar samples and the shear load-displacement curves were recorded. The UVO and UV/air (abbreviated as UVA treatment)–treated polycarbonate was bonded to 0.5-inch (1.27 cm) diameter aluminum stubs with a two-part epoxy adhesive (Vantico, Araldite 2011). Figures 11 and 12 show the peak adhesive strength for UVO and UVA samples, respectively. The untreated polycarbonate has a bond strength of *ca.* 300 psi (2.07 Mpa). After UV treatment, no statistically significant change in the adhesive strength was observed for treatments up to 120 s. Increased adhesive bond strengths were expected from UV-treated samples because of the increase in work of adhesion and surface energy. It has been reported in the literature that UV treatment of polymers can lead to the formation of low-molecular-weight (LMW) fragments on the surface due to chain scission [16,17]. LMW fragments are typically loosely bonded to the surface and can be washed away with weak solvents such as water or ethanol. The presence of weak LMW material at the interface can interfere

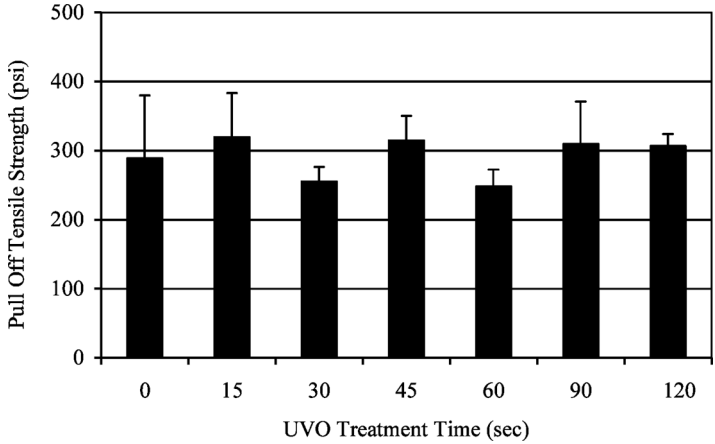

FIGURE 11 Adhesive strength of UVO-treated PC with epoxy adhesive.

with adhesion by creating a weak boundary layer that fails under low loads. Adhesion test samples were prepared using UV-treated PC, which was rinsed in ethanol prior to bonding. The effect of ozonation (no UV irradiation) was also studied for unwashed and ethanol-washed PC. Figure 13 shows the results for ozonated and UVO-treated samples before and after washing. As in the case of previous results, no significant changes in adhesion were observed.

Shear tests were performed to address the possibility of debonding between the PC film and the rigid backing to which it is attached during

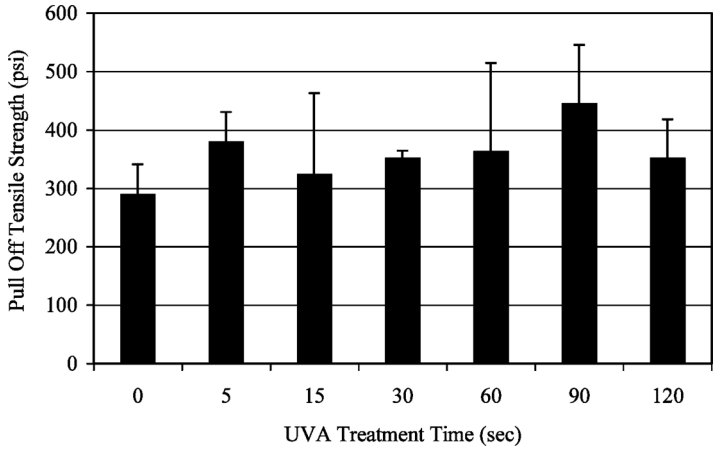

FIGURE 12 Adhesive strength of UVA-treated PC with epoxy adhesive.

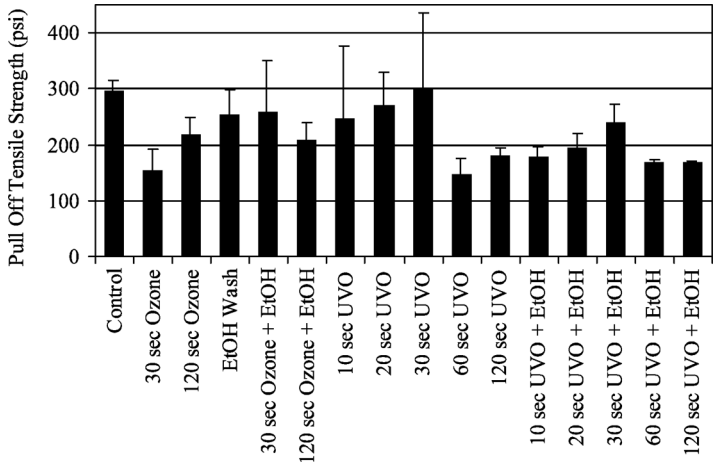

FIGURE 13 Adhesive strength of ozonated and UVO-treated polycarbonate before and after ethanol wash to remove low-molecular weight material.

tensile testing. Such debonding can lead to the development of peeling forces, which can reduce bond strengths. Shear test load-displacement curves were used to determine the adhesive bond stiffness and peak failure loads. Figure 14 shows the shear bond stiffness for UVO- and UVA-treated samples bonded with epoxy (Vantico, Araldite 2011). As in the case of tensile tests, no statistically significant changes in adhesion bond stiffness and peak failure loads were observed.

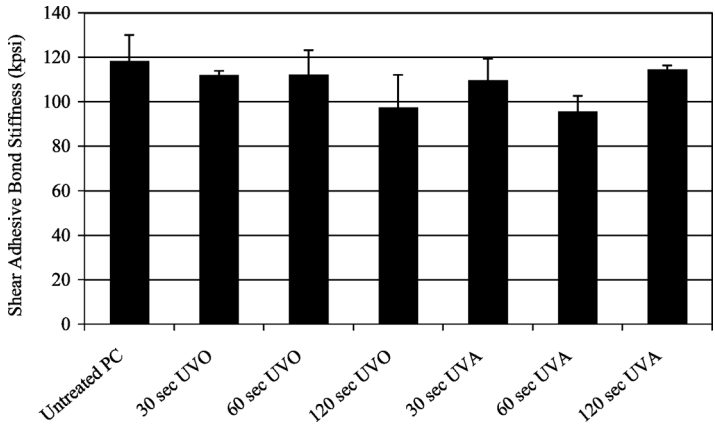

FIGURE 14 Shear adhesive bond stiffness for UVO-treated polycarbonate calculated from the slopes of load displacement curves for stub-shear adhesion tests.

The locus of failure of the adhesive bonds was investigated by fracture surface analysis using XPS. During testing, failure of the bond was found to consistently occur near the polycarbonate–epoxy interface. The two fracture surfaces generated are referred to as polycarbonate-side and epoxy-side fracture surfaces. XPS analysis of the polycarbonate-side fracture surface showed a surface resembling untreated polycarbonate even in UV-treated samples. Analysis of the epoxy-side fracture surface provided an insight into the failure mode of the UVO-treated PC–epoxy bond. The amine-cured epoxy adhesive has a unique nitrogen peak, which is absent in polycarbonate. Table 4 shows the atomic composition of cured epoxy adhesive, polycarbonate, and the adhesive-side fracture surfaces for untreated and UVO-treated PC–epoxy adhesive test samples. Three samples were analyzed for each condition to ensure accuracy. The cured epoxy has 8.5% nitrogen and 6.1% oxygen on the surface. The adhesive-side fracture surfaces have a much lower nitrogen concentration ranging from 3 to 4% and a higher oxygen concentration between 12 and 15%. The compositions of the fracture surfaces were identical within experimental error for untreated PC, UVO-treated PC, and UVO-treated PC samples rinsed in deionized water to remove LMW material from the surface prior to bonding. The composition of the adhesive-side fracture surface is consistent with the presence of a thin layer of polycarbonate on top of the epoxy adhesive. The nitrogen tag atom on the epoxy allows further quantification by using the C/N ratio of the pure epoxy to attribute part of the total carbon signal from the fracture surfaces to carbon atoms in the epoxy. Using this methodology, the amount of C1s signal attributable to epoxy was calculated

TABLE 4 Atomic Composition and Analysis of Adhesion Test Fracture Surfaces (Adhesive Side) for UVO-Treated Polycarbonate–Epoxy Bonds

Surface	C (%)	N (%)	O (%)	C/N Ratio	Epoxy (%)	PC (%)
Baseline epoxy	85.4 ± 0.3	8.5 ± 0.2	6.1 ± 0.3	10.1 ± 0.2	100	0
Baseline polycarbonate	85.4 ± 1.4	0	14.5 ± 1.4	0	0	100
0-s UVO PC–epoxy failure surface	82.0 ± 3.1	3.2 ± 0.8	14.8 ± 2.4	27.2 ± 8.1	39 ± 11	61 ± 11
30-s UVO PC–epoxy failure surface	83.1 ± 1.1	3.6 ± 0.9	13.3 ± 0.6	23.8 ± 5.3	44 ± 11	56 ± 11
120-s UVO PC–epoxy failure surface	81.8 ± 2.7	4.0 ± 1.0	14.3 ± 1.9	21.5 ± 5.6	49 ± 14	51 ± 14
120-s UVO + water rinsed PC–epoxy failure surface	84.9 ± 2.0	3.0 ± 0.7	12.1 ± 1.3	29.4 ± 8.1	36 ± 8	64 ± 8

and is shown in Table 4. The remainder of the carbon signal is attributed to polycarbonate. The results show that the epoxy-side fracture surface, within the XPS sampling depth, is composed of 50–60% polycarbonate for all samples irrespective of surface treatment or removal of LMW material by washing. The percentage of polycarbonate may be slightly overestimated if the polycarbonate is present in the form of a continuous film on the adhesive surface because of the higher bias for the topmost surface layers. In all cases, it was observed that UV treatment did not change the amount of polycarbonate removed by the epoxy during bond failure.

The fracture surface analysis indicates that failure occurs approximately within the top 30–60 Å of the polycarbonate surface irrespective of UV treatment or removal of any LMW polymer formed by UVO oxidation. Such failures are indicative of a weak boundary layer within the substrate or very high interfacial adhesion, which forces the locus of failure into the relatively weaker substrate. This model of cohesive substrate failure also explains the invariance of adhesive bond strength after surface treatment. The results from nanoindentation tests show a slight increase in the modulus of UVO-treated polycarbonate in the top 500 nm of the surface, but this increase may be inconsequential if bond failure is caused by a weak boundary layer near the PC surface.

4. CONCLUSIONS

The surface treatment of polycarbonate by UV oxidation was characterized by wettability and surface energy measurements. UV exposure in ozone and air was found to impart strong hydrophilic nature to the normally hydrophobic PC surface. UV process variables such as the ozone flow rate were carefully chosen to avoid mass transfer limitations, and under these conditions, it was found that the UV modification was independent of the ozone concentration in the treatment environment. The most important process parameter was found to be the UV irradiance. The changes occurring in the polymer are strongly dependent on the total irradiant energy, or irradiation, incident on the surface, which makes the UV-treatment process independent of the exposure time. Short exposures at high irradiances and long exposures at low irradiance levels were found to yield identical surface properties (wettability, work of adhesion, and surface energy) when irradiances were varied from 1.6 to 7.5 mW/cm^2.

The mechanical properties of the modified surface were probed by nanoindentation tests. UVO-treated PC showed an increase in the modulus in the top 500 nm with increasing UV irradiation. This is

expected to be a result of UV-irradiation-induced cross-linking in the near-surface material. Despite the increase in surface modulus, adhesion tests showed no change in the adhesive bond strength with epoxy and polyurethane adhesives. Fracture surface analysis of the epoxy–polycarbonate adhesive bond using XPS showed the removal of approximately 30–60 Å of polycarbonate material by the epoxy adhesive. The cohesive failure in the substrate may be indicative of a weak boundary layer within the polycarbonate, surface or a very high level of interfacial adhesion between the epoxy and polycarbonate, which forces the locus of failure into the relatively weaker polycarbonate.

REFERENCES

[1] Mahlberg, R., Nieme, H. E. M., Denes, F., and Rowell, R. M., *International Journal of Adhesion and Adhesives* **18**, 283–297 (1998).
[2] Gutowski, W. S., Wu, D. Y., and Li, S., *J. Adhesion* **43**, 139–155 (1993).
[3] Sohn, S., Chang, S., and Hwang, I., *J. Adhesion Sci. Technol.* **17**, 453–469 (2003).
[4] Martinez-Garcia, A., Sanchez-Reche, A., Gisbert-Soler, S., Cepeda-Jiminez, C. M., Torregrosa-Macia, R., and Martin-Martinez, J. M., *J. Adhesion Sci. Technol.* **17**, 47–65 (2003).
[5] Strobel, M. and Lyons, C. S., *J. Adhesion Sci. Technol.* **17**, 15–23 (2003).
[6] Sako, N., Matsuoka, T., and Sakaguchi, K., *Composite Interfaces* **4**, 401–415 (1997).
[7] Strobel, M., Walzak, M. J., Hill, J. M., Lin, A., Karbashewski, E., and Lyons, C. S., *J. Adhesion Sci. Technol.* **9**, 365–383 (1995).
[8] Kruse, A., Kruger, G., Baalmann, A., and Hennemann, O. D., *Polymer Surface Modification: Relevance to Adhesion* (Brill Academic Press, Leiden, 1996), pp. 291–301.
[9] Lane, J. M. and Hourston, D. J. *Progress in Organic Coatings* **21**, 269–284 (1993).
[10] Bhurke, A. S. and Jensen, M. *UV Treatment — A Low Cost, Environmentally Friendly Surface Treatment Technique* (ML890 Report, Case Center for Computer-Aided Engineering and Manufacturing, East Lansing, 1997).
[11] Hashem, T. M., Zirlewagen, M., and Braun, A. M., *Wat. Sci. Tech.* **35**, 41–48 (1997).
[12] Macmanus, L. F., Walzak, M. J., and Mcintyre, N. S., *Journal of Polymer Science: Part A: Polymer Chemistry* **37**, 2489–2501 (1999).
[13] Kesting, W., Knittel, D., Bahmers, T., and Schollmeyer, E. *Applied Surface Science* **54**, 330–335 (1992).
[14] Buchman, A., Dodiuk, H., Rotel, M., and Zahavi, J. *Polymer Surface Modification: Relevance to Adhesion* (Brill Academic Press, Leiden, 1996), pp. 199–212.
[15] Sancaktar, E., Babu, S. V., Zhang, E., and D'Couto, G. C., *J. Adhesion* **50**, 103–133 (1995).
[16] Bolle, M. and Lazare, S., *Applied Surface Science* **54**, 471–476 (1992).
[17] Krajnovich, D. J., *J. Phys.Chem. A* **101**, 2033–2039 (1997).
[18] Walzak, M. J., Flynn, S., Foerch, R., Hill, J. M., Karbashewski, E., Lin, A., and Strobel, M., *Polymer Surface Modification: Relevance to Adhesion* (Brill Academic Press, Leiden, 1996), pp. 253–272.
[19] Peeling, J. and Clark, D. T., *Journal of Polymer Science: Polymer Chemistry Edition* **21**, 2047–2055 (1983).
[20] Charbonnier, M., Romand, M., Esrom, H., and Seebock, R., *J. Adhesion* **75**, 381–404 (2001).

[21] Praschak, D., Bahners, T., and Schollmeyer, E., *Appl. Phys. A.* **66**, 69–75 (1998).
[22] Pasternak, M., *Journal of Applied Polymer Science* **57**, 1211–1216 (1995).
[23] Minagawa, M., Saito, T., Fujikura, Y., Watanabe, T., Iwabuchi, H., Yoshii, F., and Sasaki, T., *J. Appl. Polym. Sci.* **63**, 1625–1633 (1997).
[24] Yu, J. R., Chen, Z. L., Zhu, J., Liu, Z. F., and Wang, Q. R., *Intern. Polymer Processing* **14**, 331–335 (1999).
[25] Petit, S., Laurens, P., Barthes-Labrousse, M. G., Amouroux, J., and Arefi-Khonsari, F., *J. Adhesion Sci. Technol.* **17**, 353–368 (2003).
[26] Romero-Sanchez, M. D., Pastor-Blas, M. M., Martin-Martinez, J. M., and Walzak, M. J., *J. Adhesion Sci. Technol.* **17**, 25–45 (2003).
[27] Ouyang, M., Yuan, C., Muisener, R. J., Boulares, A., and Koberstein, J. T., *Chem. Mater.* **12**, 1591–1596 (2000).
[28] Kavc, T., Kern, W., Ebel, M., Svagera, R., and Polt, P., *Chem. Mater.* **12**, 1053–1059 (2000).
[29] Grujicic, M., Cao, G., Rao, A. M., Tritt, T. M., and Nayak, S., *Applied Surface Science* **214**, 289–303 (2003).
[30] Dontula, N., Weitzsacker, C., and Drzal, L. T., *Proc. 20th Annual Meeting of the Adhesion Society* (Adhesion Society, Blacksburg, VA, 1997) 97–99.
[31] Rabek, J. F., *Mechanisms of Photophysical Processes and Photochemical Reactions in Polymers* (Wiley, New York, 1987).
[32] Crawford, R. J., *Plastics Engineering*, 2nd ed. (Pergamon Press, New York, 1987).
[33] Soloukhin, V. A., Brokken-Zijp, J. C., VanAsselen, O., and DeWith, G. *Macromolecules* **36**, 7585–7597 (2003).
[34] Good, R. J. *J. Adhesion Sci. Technol.* **6**(12), 1269–1302 (1992).
[35] VanOss, C. J., Good, R. J., and Chaudhury, M. K. *J. Colloid Interface Sci.* **111**, 378 (1986).